Spring 2023

Remote Sensing of Riparian Areas and Invasive Species

Molly E. Yanchuck
University of New Hampshire, Durham

REMOTE SENSING OF RIPARIAN AREAS AND INVASIVE SPECIES

BY

MOLLY E. YANCHUCK

Bachelor of Science, Geoenvironmental Studies, Shippensburg University 2017

THESIS

Submitted to the University of New Hampshire in Partial Fulfillment of the Requirements for the Degree of

Master of Science

in

Natural Resources: Environmental Conservation and Sustainability

May 2023

This thesis has been examined and approved in partial fulfillment of the requirements for the degree of Master of Science in Natural Resources: Environmental Conservation and Sustainability by:

Dr. Russell G. Congalton, Thesis Co-Chair,
Remote Sensing and Geographic Information Systems,
Natural Resources and the Environment

Dr. John S. Gunn, Thesis Co-Chair
Affiliate Research Assistant Professor,
Natural Resources and the Environment

Dr. Benjamin T. Fraser,
Natural Resources and the Environment

On April 17th, 2023

Approval signatures are on file with the University of New Hampshire Graduate School.

ACKNOWLEDGEMENTS

I would firstly like to thank my advisor, Dr. Russell G. Congalton, for taking me on as a graduate student. This opportunity has changed my life. Your mentorship exceeded your academic expertise in remote sensing and geospatial analysis. It was your never-ending enthusiasm and patience for your students, me especially, that made this experience as impactful as it was. I would also like to give a big thank you to my committee co-chair, Dr. John S. Gunn, who provided the funding necessary to complete this research. In addition to your financial support, I appreciated your kindness and assistance with fieldwork. To my lab mate and committee member, Dr. Benjamin T. Fraser, thank you for your guidance, teaching me how to fly, and always being available for the long drive to Lancaster.

Thank you to all my lab mates, Jianyu Gu, Heather Grybas, Sarah Reny, and Christine Bunyon, for your comradery. Grad school is much less lonely when you're a part of a team, and I couldn't have asked for a better bunch. I'm especially grateful for Heather Grybas, who has shown me the way since day one. Thank you for all your help with my various technical issues, always being there to listen, introducing me to dark beers, picking me up when I was down, and most of all, for your friendship.

Thank you to my family for your love and support, especially my parents, Gregory and Beth Ann Yanchuck. Thank you for raising me to follow my dreams, and for cheering me on every step of the way. The distance between us may be great, but the love we share is greater! Thank you to Reed Laakso for everything you've done to support me through these last two years. You've helped me grow into stronger a stronger version of myself. Thank you to Katrina Shoemaker for your years of friendship, and for always being there to motivate or inspire. Your encouragement led me to apply to graduate school, and I am forever grateful. This journey wouldn't have been the same without all of you.

TABLE OF CONTENTS

LIST OF TABLES

LIST OF FIGURES

ABSTRACT

REMOTE SENSING OF RIPARIAN AREAS AND INVASIVE SPECIES

by

Molly E. Yanchuck

University of New Hampshire, May 2023

Riparian areas are critical landscape features situated between terrestrial and aquatic environments, which provide a host of ecosystem functions and services. Although important to the environmental health of an ecosystem, riparian areas have been degraded by anthropogenic disturbances. These routine disturbances have decreased the resiliency of riparian areas and increased their vulnerability to invasive plant species. Invasive plant species are non-native species which cause harm to the ecosystem and thrive in riparian areas due to the access to optimal growing conditions.

Remote sensing provides an opportunity to manage riparian habitats at a regional and local level with imagery collected by satellites and unmanned aerial systems (UAS). The aim of this study was two-fold: firstly, to investigate riparian delineation methods using moderate resolution satellite imagery; and secondly, the feasibility of UAS to detect the invasive plant *Fallopia japonica* (Japanese Knotweed) within the defined areas. I gathered imagery from the Landsat 8 OLI and Sentinel-2 satellites to complete the regional level study and collected UAS imagery at a study site in northern New Hampshire for the local level portion. I obtained a modest overall accuracy from the regional riparian classification of 59% using the Sentinel-2

imagery. The local invasive species classification yielded thematic maps with overall accuracies of up to 70%, which is comparable to other studies with the same focus species. Remote sensing is a valuable tool in the management of riparian habitat and invasive plant species.

CHAPTER I:

REMOTE SENSING, INVASIVE SPECIES, AND RIPARIAN AREAS

1.1 Invasive Plant Species

Throughout history and to present day, humans have aided in the global redistribution of plant species. The majority of non-native species have been intentionally introduced to new ranges as ornamentals for horticultural purposes, while others were cultivated for agricultural and forestry applications (Finch et al., 2021; Lehan et al., 2013; Richardson and Rejmánek, 2011; Bradley, 2010). In some cases, these species escape their enclosures and become established colonies. Additionally, some species have been unintentionally introduced to areas through contaminated seed and soil (Lehan et al., 2013). A non-native (alien) species is not always considered to be invasive. As defined by the Executive Order 13112 of 1999, an invasive species is an alien species that causes harm to the ecology and economy of the new ecosystem (Exec. Order No. 13112, 1999). In the United States, there are an estimated 5,000 non-native plant species growing in natural ecosystems, compared to an estimated 17,000 native plant species (Finch et al., 2021; Pimentel et al., 2000).

Invasive plant species are often able to outcompete native flora for resources and space, allowing them to establish colonies and rapidly spread throughout an area. The success of an invasion is dependent on the physiological characteristics of the species as well as the environmental characteristics of the ecosystem (Hess et al., 2019; Vila and Weiner, 2004). Invasive species possess beneficial mechanisms such as an elevated nutrient uptake, extended leaf phenology, differential timing of resource use in comparison to native flora, resistance to herbivores, and biochemical mechanisms (i.e., allelopathy) (Allen et al., 2013; Levin et al., 2003; Tickner et al., 2001). The ecosystems which are most susceptible to colonization experience

routine natural or anthropogenic disturbances (Richardson et al., 2011). Additionally, as climate change is expected to increase the frequency and intensity of natural disasters (e.g., floods, droughts), invasive species are predicted to benefit from these disturbances and further their spread.

The consequences of colonization by invasive plant species are numerous. They greatly impact the composition of native flora, as invasions cause a decrease in native species richness and diversity, as well as risk the extinction of threatened or endangered species (Kumar Rai & Singh, 2020; Hayes & Holzmueller, 2012; Hejda et al., 2009). Invasive plant species also affect ecosystem functions by altering and accelerating nitrogen and carbon cycles, which promotes plant growth and spread (Allen et al., 2013; Levine et al., 2003). Furthermore, invasives can alter hydrologic regimes through water consumption and changing the rate or timing of evapotranspiration and runoff (Ehrenfeld, 2010). Economically, invasive species cause harm by reducing land value and causing billions in damages and control costs annually (Mayfield et al., 2021). It is for these reasons that it is increasingly important to investigate methods to effectively manage invasive species.

The current methods implemented in the United States to manage invasions are firstly, prevention through the monitoring of intentionally imported species, secondly, early detection and rapid response (EDRR), and thirdly, containment, eradication, and control (Westbrooks, 2004; Rejmánek, 2000). EDRR is accomplished by locating invasive species shortly after establishment and prior to a widespread invasion, and quickly acting to remove the species from the invaded habitat. Detection is often completed through ground surveying and predictive distribution models. Ground surveys are completed by either professional field crews or citizen-based volunteer groups (Reaser, 2020; Westbrooks, 2004). Although ground surveys are an

important component to invasive species management, they are time consuming and costly. Citizen-based surveying can produce valuable results, but can often be variable in quality, decreasing the usefulness of the data for analysis and modeling (Oswalt et al., 2021; Crall, 2010). Therefore, additional methods, such as remote sensing, are required for effective invasive species management.

1.2 Remote Sensing Characteristics and Platforms

Remote sensing is the process of obtaining information about an object or phenomena without physical contact (Jensen, 2016; Huang & Asner, 2009). It is an advantageous tool that is cost-effective, provides a synoptic view of landscapes, covers large spatial extents, and yields multitemporal and multispectral data (Joshi & Duren., 2004). Thus, remote sensing allows for rapid data collection and frequent analyses, especially of environments that are difficult to access on the ground. Remotely sensed data (i.e., digital images) are collected by three primary platforms: satellites, manned aircraft, and unmanned aerial systems (UAS). Each platform is equipped with sensors that differ in their spatial, spectral, radiometric, and temporal resolutions, as well as their extent. Therefore, each data product will have different characteristics and platform selection must be given due consideration.

Spatial resolution, or the ground sampling interval, is a measure of the smallest pixel that can be detected by the sensor (Jensen, 2016; Huang & Asner, 2009). The government-operated Landsat 8 Operational Land Imager (OLI) and Sentinel-2 have a respective spatial resolution of 15 to 30 meters, and 10 to 20 meters. In comparison, commercial satellites can obtain a spatial resolution up to 0.5 meters (Toth and Jóźków, 2016). These resolutions are similar to those captured by aerial imagery. Currently, the highest spatial resolution images are captured by UAS, which have a resolution as fine as a few centimeters or less (Manfreda, 2018).

Spectral resolution is the number and width (nanometers) of wavelengths that can be detected by a sensor (Jensen, 2016). These wavelengths are often referred to as bands (e.g., band 1 on Landsat thematic mapper is called the blue band). Remote sensing systems can collect panchromatic, normal color, multispectral, and hyperspectral information. Panchromatic images consist of a single, wide, band of the entire visible spectrum. Normal color sensors detect bands in visible light separated into blue, green and red (B, G, R). Multispectral images consist of multiple narrow bands, such as visible B, G, R), near-infrared (NIR), middle-infrared (MIR), thermal-infrared (TIR), and red-edge wavelengths. Hyperspectral images consist of hundreds of continuous, narrow spectral bands. Spectral bands can be combined to conduct further analyses on an image in a technique known as band ratioing, or indices. A common index is the Normalized Difference Vegetation Index (NDVI), which is used to indicate vegetation health and is calculated using the red and near-infrared (NIR) bands: (NIR- Red)/(NIR + Red) (Jensen, 2016; Fu and Burgher, 2015).

The temporal resolution is determined by how often the sensor revisits an area and varies between platforms. Satellites, both commercial and government-operated, have a low temporal resolution as they are limited by their orbits. Some satellites capture imagery more frequently than others. For example, Landsat 8 OLI and Sentinel-2 have temporal resolutions of 16 and 5 days, respectively. Satellites can increase their temporal resolution by tilting their sensors to capture imagery off-nadir, but are ultimately limited by their orbit (Jabari and Krafczek, 2019). Both manned and unmanned aerial systems have the potential for higher temporal resolution, as they are not limited by a pre-set orbit, and can collect imagery as often as weather conditions and funding allow. However, commercially operated manned aerial flights are expensive and government-operated manned aerial flights, such as the National Agriculture

Imaging Program (NAIP), only collect data every three years (Manfreda, 2018). Therefore, UAS are the remote sensing platform that is both accessible and offers a high temporal resolution.

Radiometric resolution is the sensitivity of the sensor to received electromagnetic energy (i.e., reflectance) and influences its ability to discriminate between signal levels (i.e., shades of grey) (Jensen, 2016). The reflectance information captured by sensors are stored as a digital number value from 0 to 2^n in a pixel, with n being the number of bits the sensor used to collect the data. For example, 8-bit imagery has 256 (2^8) potential shades of grey ranging from 0 to 255. Images composed of more bits have a higher radiometric resolution and are more likely to detect subtle spectral changes. Currently, the maximum data that a sensor can collect is 14-bits, or 16,384 (2^{14}) shades and is stored in a 16-bit format (Verde et al., 2018).

The final characteristic of remote sensing platforms is the extent of the sensor. The extent, or footprint, is the scene that is captured by the sensor. The size, scale, and direction of the scene is dependent on the remote sensing platform. Satellite sensors can capture hundreds of thousands of square kilometers in a single scene. For example, the Landsat 8 OLI sensor captures a scene that is 170 kilometers (north-south) by 183 kilometers (east-west). In comparison, UAS would require several flights to capture a fraction of the extent.

Each of the characteristics of remotely sensed data must be taken into consideration prior to analysis, as there are some trade-offs between characteristics. Spatial and spectral resolutions have an inverse relationship. Landsat 8 OLI has a 30-meter resolution for bands 1 through 7 and band 9 and 15-meter resolution for band 8. Bands 1 through 7, and 9 are multispectral bands, while band 8 is panchromatic. Panchromatic images have a higher spatial resolution but a lower spectral resolution because they are portrayed in greyscale. Multispectral images have a lower spatial resolution but a higher spectral resolution because they are portrayed

in color. Spatial resolution also has an inverse relationship to temporal resolution. Typically, higher resolution imagery are captured less frequently than lower resolution images (Jensen, 2016). The relationship is dependent on the remote sensing platform and is most applicable to satellite and manned aerial imagery. However, this relationship is less applicable to UAS, which are the most temporally flexible platform.

1.2.1 Remote Sensing Data Products

In order to transform remote sensing data into products, imagery must undergo digital image processing. Digital image processing is a means to interpret and analyze imagery, and encompasses a variety of processes, such as classification (Lillesand et al., 2015). Image classification is the process where imagery is transformed into a thematic map which displays the location of user-defined classes. To accomplish an image classification, the user must first create a well-defined classification scheme that is hierarchical, totally exhaustive, and mutually exclusive (Congalton and Green, 2019). These parameters ensure that the entire image is labeled into the chosen thematic classes. Historically, images were classified manually by an analyst using the elements of image interpretation: size, shape, texture, pattern, shadow, tone, and site (Jensen, 2016). This approach, however, has its disadvantages as it is limited to the visual characteristics of image objects, the knowledge of the analyst, and the abilities of the human eye to fully detect spectral characteristics. Presently, digital images are classified using digital image processing software, which can utilize spectral information and analyze a greater amount of imagery (Lillesand et al., 2015).

Image processing software, such as eCognition, classifies pixels of imagery through spectral pattern and spatial pattern recognition (Hossain & Chen, 2019). Spectral pattern recognition assigns pixels with similar reflectance values to the same class. Spatial pattern

recognition groups pixels based on their proximity to similar pixels which share characteristics such as texture, size, shape, direction, and context (Lillesand et al., 2015). These procedures are the basis of the primary methods of image classification: pixel-based classification (PBC) and object-based image analysis (OBIA) (Lillesand et al., 2015; Gao and Mas, 2008). PBC solely employs the spectral pattern recognition procedure and labels individual pixels based on their reflectance values. In contrast, OBIA incorporates both spectral and spatial procedures to create image objects (i.e., groups of homogenous pixels).

Traditionally, PBC was the chosen method of image classification, as OBIA was difficult to implement due to the coarse resolution of early imagery and the computational limitations of hardware. The advancement of hardware processing capabilities and increased accessibility to high and very high-resolution imagery has since led to the widespread adoption of OBIA (Sibaruddin et al., 2018; Gao and Mas, 2008). The OBIA method consists of two steps: segmentation and classification. The segmentation process dissects the image into polygons composed of homogenous pixels known as image objects. The most commonly used segmentation technique is the multiresolution segmentation (MRS) algorithm, which is proprietary to the eCognition software (Cánovas-García & Alonso-Sarría, 2015). MRS is a bottom-up region merging technique that begins by considering each individual pixel as a unique object, then merges pairs of objects together to form larger segments (Rahman and Saha, 2008; Karakış et al., 2006). The decision to merge objects is determined by the homogeneity criterion which is composed of color (spectral values) and shape (smoothness and compactness). The merging process ends when the scale parameter threshold is met or exceeded. The scale parameter defines the maximum amount of heterogeneity permitted within the image objects, and subsequently, affects the average size of the objects. A low scale parameter value allows for

a low amount of heterogeneity among image objects, which creates objects that are composed of fewer pixels and therefore, are smaller than if the scale parameter was set to a higher threshold (Rahman & Saha, 2008; Tian & Chen, 2007). Although time consuming, these parameters are typically optimized through trial and error (Saba et al., 2013).

After the image is segmented, the newly created image objects are classified. There are a variety of classification algorithms that can be used to assign the objects to a thematic class. Recently, machine learning algorithms (MLA) have become popular alternatives to traditional parametric classifiers because they are non-parametric and therefore do not rely on normal data distributions, can handle complex data, and produce results with higher accuracies (Maxwell et al., 2018; Rodriguez-Galiano et al., 2012). In particular, ensemble MLAs have gained attention for being more robust and accurate than single ML classifiers (Jensen, 2016). Starting from a base classifier, ensemble algorithms create, then aggregate multiple iterations of a classification with random samples from the training data (Rodriguez-Galiano et al., 2012). A common ensemble MLA used in land cover classification is Random Forests (RF). A study by *Rodriguez-Galiano et al.,* (2012) noted the various advantages of RF which most importantly included the classifier's robustness to noise and outliers in the training data, a low sensitivity to training data size, ability to generate an unbiased error estimate, and is computationally efficient. The RF classifier is an ensemble of decision trees, which are grown to the greatest extent without pruning (e.g., removing redundancies), using about 70% of the training data that has been randomly selected, and reserving about 30% of the data to determine the generalization error (Jensen, 2016; Breiman, 2001). The generalization error is a measure of how accurately the algorithm can classify new data. Once the user-determined number of trees are created, the unclassified objects are given to the forest, and each tree "votes" to assign the object to one of the user-defined

classes. The forest determines the final classification of the object by assigning it to the class with the most "votes" from the trees (Jensen, 2016; Breiman, 2001).

1.2.2 Accuracy Assessment

Historically, the accuracy of a thematic map was assessed with a subjective approach, often determined by how correct the final product appeared, or was given no consideration at all (Congalton, 1991). Over time objective and qualitative methods have been developed. Presently, accuracy is most commonly measured using an error matrix (Rwanga & Ndambuki, 2017). An error matrix, also known as a confusion matrix or contingency table, compares the agreement and disagreement between the reference data and the classified data (Congalton and Green, 2019). Reference data (i.e., validation data) are samples which have a known land cover class and are obtained through ground data collection or image interpretation. The reference data are represented as columns, while classified data are represented as rows. The sample units are entered into the matrix based on its known land cover class and the assigned map class. The major diagonal in the matrix displays the agreement between the reference and classified data (Story and Congalton, 1986). An error matrix can be used to calculate three accuracy statistics: overall, user's, and producer's (Story and Congalton, 1986). The overall accuracy is the most commonly reported statistic, and is calculated by dividing the sum of the major diagonal and the total number of reference data samples (Congalton and Green, 2019). Overall accuracy represents the accuracy of the entire map, while user's and producer's accuracy provide information about how accuracy is distributed throughout the map classes (Story and Congalton, 1986). User's accuracy represents commission error, or error of inclusion, which is the probability that a sample was assigned to the incorrect map class. It is calculated by dividing the major diagonal value for each class (i.e. the correctly classified samples) by the total number of

samples that were classified as that class (Congalton and Green, 2019; Story and Congalton, 1986). Producer's accuracy represents omission error, or the error of exclusion, which is the probability that a sample was misassigned from its correct map class. It is calculated by dividing the major diagonal value of each class by the total number of reference samples for the specific class (Congalton and Green, 2019; Story and Congalton, 1986).

1.3 Riparian Areas

Riparian areas are critical landscape features, which serve as an ecotone between aquatic and terrestrial environments (Michez et al., 2016; Rahe et al., 2015; Vidon et al., 2010). They are the area of land between a surface water body (e.g., stream) and the concurrent hillslope, encompassing the floodplain and some upland areas (McGlynn & Seibert, 2003). Although riparian areas are often narrow and cover a small area, they perform critical ecosystem functions and services such as habitat for both terrestrial and aquatic organisms, shade to regulate surface water temperature, and provide bank stability (Vidon et al., 2010). They also influence the hydrologic flow paths of surface and subsurface flows, acting as an intermediate zone before flows reach the adjacent surface water body; allowing the riparian areas to filter nutrients, and buffer uplands from floodwaters.

Despite riparian areas being ecologically and hydrologically significant, they are one of the most anthropogenically disturbed habitats across the globe (Liendo et al., 2015). These disturbances are historical, as humans have settled along waterways for centuries and have intensely modified the environment through changes in land use (e.g. agriculture), physical alterations to the landscape (e.g. deforestation, dams, roads, channel straightening), and lowering of water tables (Michez et al., 2016; Liendo et al., 2015; Naiman and Decampes, 1997). The routine disturbance to riparian ecosystems ultimately reduces their resiliency and increases their

vulnerability to erosion, pollution, and, specifically, invasive species (González del Tánago and García de Jalón, 2006). Invasive species thrive in riparian areas due to the water availability and dynamic hydrology, as flooding events create opportunities to dislodge established species, and disperse seeds or propagules for reproduction (Michez et al., 2016; Tickner et al., 2001). According to a 2008 national assessment of freshwater resources, 62% of riparian plant communities are at risk of being lost (Vanderklein et al., 2014). The assessment also reported that the United States has seen an increase of groundwater removal of 46% since 1960 (Vanderklein et al., 2014). Riparian areas are reliant on hydrologic flows, and therefore require water availability. As the climate changes, the United States is expected to experience an increase in evaporative demands and a decrease in streamflow; both of which will impact the availability of groundwater. These changes can then impact the composition of the vegetation, endangering the native flora, and increasing the possibility of invasion. The protection and restoration of riparian vegetation and habitat require an inventory of current conditions and can be accomplished by using remote sensing (Congalton et al., 2002).

1.4 Riparian Delineation and Mapping

To manage and preserve riparian areas, they must be identified and mapped. Remote sensing, especially when combined with a geographic information system (GIS), are invaluable to this process. Presently, there is not a standard method to delineate the extent of a riparian area from its adjacent waterbody (de Sosa et al., 2018). Methods often follow either a fixed-width buffer or variable-width approach. The fixed-width buffer approach delineates a riparian area based on a single distance from the waterbody. The width distance varies among studies and is often influenced by different variables such as the stream order (Yang, 2007) or governmental recommendations (Congalton et al., 2002). The variable-width approach utilizes ancillary

information, such as digital elevation models (DEM), flood heights, and soil characteristics, to create a buffer (de Sosa et al., 2018). Although the fixed-width approach is simpler to implement, studies by *Salo et al.,* (2016) and *de Sosa et al.,* (2018) have found that the variable-width approach yields more accurate results when estimating the extent of a riparian area.

Remotely sensed imagery has been used to map riparian areas and vegetation with varying levels of success. Mapping is often completed using publicly available satellite imagery because the data is routinely collected, encompasses large areas, and is more cost-effective than commercial satellites or aerial photography (Congalton et al., 2002). Although common sources, these satellites often have moderate spatial resolutions of 10 meters (e.g., Sentinel-2) or larger, (e.g., Landsat 8 OLI, 30 meters) and are therefore limited in their ability to accurately map riparian areas because they are often narrow, linear features that consist of heterogeneous vegetation (Johansen et al., 2010; Congalton et al., 2002). Therefore, a few pixels could represent the entire segment of a riparian buffer which poses a challenge when classifying and mapping riparian vegetation, as multiple vegetation types are combined within the same pixel, creating spectral confusion. There have been several suggested approaches in the literature to improve riparian vegetation mapping with moderate resolution satellite imagery. *Congalton et al., 2002* proposed that riparian and upland vegetation be sampled separately due to the differences in vegetation types. Studies such as *Baker et al., 2006* and *Villarreal et al., 2012* have had success with this approach, obtaining accuracies of 73% and 86%, and 91% and 87% respectively. Although these classifications are not at a species level, they proved useful for differentiating between riparian and non-riparian vegetation communities. These differences can further be explored with vegetation indices, such as normalized difference vegetation index (NDVI) and normalized difference water index (NDWI) which are indicators of greenness and

wetness (Barron et al, 2012; Xie et al, 2008). The study by *Barron et al.,* (2012) proposed that remote sensing can be used to identify areas of persistent greenness and wetness in dry seasons to delineate vegetation communities. The study utilized multiple dates of Landsat TM data in conjunction with NDVI and NDWI indices, yielding results from 59% to 91% producer's accuracy.

Many studies (Huylenbroeck et al., 2020; Yang, 2007; Goetz, 2006; Congalton et al., 2002) have determined that an increase in spatial resolution is required to map riparian vegetation more accurately at a species level. However, high to very high resolution data collected by either commercial satellites (WorldView, 0.6 meters; Rapideye, 5 meters) or aerial imagery cost thousands of dollars, and are not practical for continuous mapping and monitoring of riparian areas. Even if costs were eliminated, such as with the free aerial imagery collected through the National Agriculture Imagery Program (NAIP, 1 meter), the temporal resolution of three years creates another obstacle to this goal. Unmanned aerial systems (UAS) have emerged as a means to map riparian vegetation, including invasive species, at a local scale because of the platform's high spatial and temporal resolution (Huylenbroeck et al., 2020).

1.4.1 Remote Sensing of Riparian Invasive Plant Species

Due to the regular disturbance and degradation of riparian areas, they have become increasingly susceptible to invasive plant species (Michez et al., 2016). Effective management of invasions require regular monitoring which can be accomplished by using remotely sensed imagery with the appropriate spatial and temporal resolution (Müllerová et al., 2013). Early detection and rapid response (EDRR) is the optimal management approach for invasive species, and is made more feasible with UAS. Since UAS have a high temporal resolution and can be deployed as frequently as needed, they can routinely capture the same area. The high spatial resolution increases the likelihood that small patches are captured prior to a widespread invasion

and allows for the close monitoring of established colonies. In addition, the temporal flexibility of UAS allows for rapid collection of imagery during critical phenological stages when invasive plants are more distinct from other riparian vegetation through flowering or leaf-coloring (Müllerová et al., 2017; Michez et al., 2016). For example, the herbaceous invasive plant *Fallopia japonica* (Japanese Knotweed) is characterized by its red-brown stems during the autumn senescence, and white flowers during late summer (Dorigo et al., 2012).

1.5 Summary

Riparian areas are of critical ecological importance, but routine disturbance has left them susceptible to invasive plant species. Invasive plants are harmful to the overall health of riparian areas and are expected to negatively impact the ecosystem services provided by these areas. Remotely sensed satellite data can be used to define riparian areas at a regional scale but are unable to map riparian vegetation species at a finer scale. Unmanned aerial systems have the ability to detect and map vegetation to these finer scales, including invasive species. The collected imagery can then be classified into thematic maps. These products can assist land managers in understanding the extents of riparian habitat, and the locations of the invasive species within the boundaries, allowing for more precise management efforts.

CHAPTER 2:

REMOTE SENSING OF RIPARIAN AREAS AND INVASIVE SPECIES

2.1 Introduction

Riparian areas are the interface between a surface water body and the adjacent terrestrial uplands. They are important landscape features that provide a host of ecosystem functions and services such as species habitat, nutrient filtering, stream-shading, bank stability, and flood mitigation (Goetz, 2006; Naiman & Décamps, 1997). Although environmentally significant, riparian areas are one of the most anthropologically disturbed ecosystems in the world and consequently, riparian vegetation species are being lost at an alarming rate (Liendo et al., 2015; Vanderklein et al., 2014). The loss of native vegetation reduces the area's capacity to perform ecosystem functions, leading to decreased biodiversity and water quality, as well as an increased vulnerability to threats, specifically invasive species (Liendo et al., 2015). Invasive species are alien species that cause both ecological and economical harm to the ecosystem to which they've been introduced (Exec. Order No. 13112, 1999). Invasive plants in riparian areas often thrive due to the ideal growing conditions (e.g., access to water and light) and dynamic hydrology, as flooding events remove native vegetation from banks, creating space for colonization, and providing an opportunity to reproduce through hydrochory (Michez et al, 2016; Tickner et al. 2001).

Riparian management practices typically focus on the restoration of riparian vegetation due to its critical role in the ecosystem (Huylenbroeck et al., 2020). In order to promote the growth of native vegetation, it is key to control the spread of invasive plant species. Presently, best management practices in the United States first suggest prevention, then early detection

rapid response (EDRR), and finally containment, eradication, and control (Westbrooks, 2004; Rejmánek, 2000). The aim of EDRR is to locate and remove invasive plants while colonies are small and newly established. The EDRR detection process is typically implemented through ground surveys and predictive models. However, these methods are time-consuming, costly, and run the risk of further disturbing fragile ecosystems (Reaser, 2020). Therefore, it is important to investigate more efficient methods for detection, so that more resources can be allocated to the removal of the species.

Remote sensing is a valuable tool that can assist in both the management of riparian habitat and monitoring of invasive plant species. At a regional scale, riparian areas are often mapped using publicly available satellite imagery despite their moderate resolution, because the data is regularly collected, covers large extents, and is cost-effective (Congalton et al., 2002). Although these data sources are limited in their ability to map riparian vegetation at a species level, they have been used to successfully delineate riparian from non-riparian vegetation communities (e.g., uplands) (Villarreal et al., 2012; Baker et al., 2006). Species-level mapping requires high to very high-resolution imagery (< 10 m) which can be obtained through commercial satellites and/or aerial imagery, however these platforms are expensive and limit the ability to frequently map riparian areas and thus detect invasives (Huylenbroeck et al., 2020). Presently, unmanned aerial systems (UAS) provide access to high resolution imagery at a relatively low cost. Additionally, UAS have a high temporal resolution, which allows them to routinely capture images over the same area and increases the likelihood of detecting invasives prior to large-scale invasions.

In this study, I investigated the applications of remote sensing in the context of riparian habitat management at a regional and local scale. Using satellite imagery from Landsat 8 OLI

and Sentinel-2, my objective was to incorporate methods suggested by the literature to improve riparian classification with moderate resolution imagery; secondly, compare the accuracies of the different satellites; and thirdly, compare the accuracies between each season. Then using UAS imagery, I tested how accurately invasive plant species could be detected in a riparian habitat and explored whether detection was influenced by the seasonality of the imagery.

2.2 Study Area

The study area is located at Garland Brook in Lancaster, New Hampshire (44° 28' 24.32", -71° 28' 48.25"). The site parameters exist at two scales, regional and local, to fit the goals of the research (Figure 1). The regional site is slightly larger than a National Agricultural Image Program (NAIP) image, approximately 6 x 8 km with an estimated area of 48 $km^{2.}$ The site is dominated by upland and riparian forest and other vegetation types (i.e., grass and shrubs), with few urban features. Presently, the local site is adjacent to logging operations. The local site is contained within three UAS flight blocks: northern, southern, and center, measuring a respective 230 x 623, 226 x 500, 216 x 658 meters and covering a total area of 0.4 km^2.

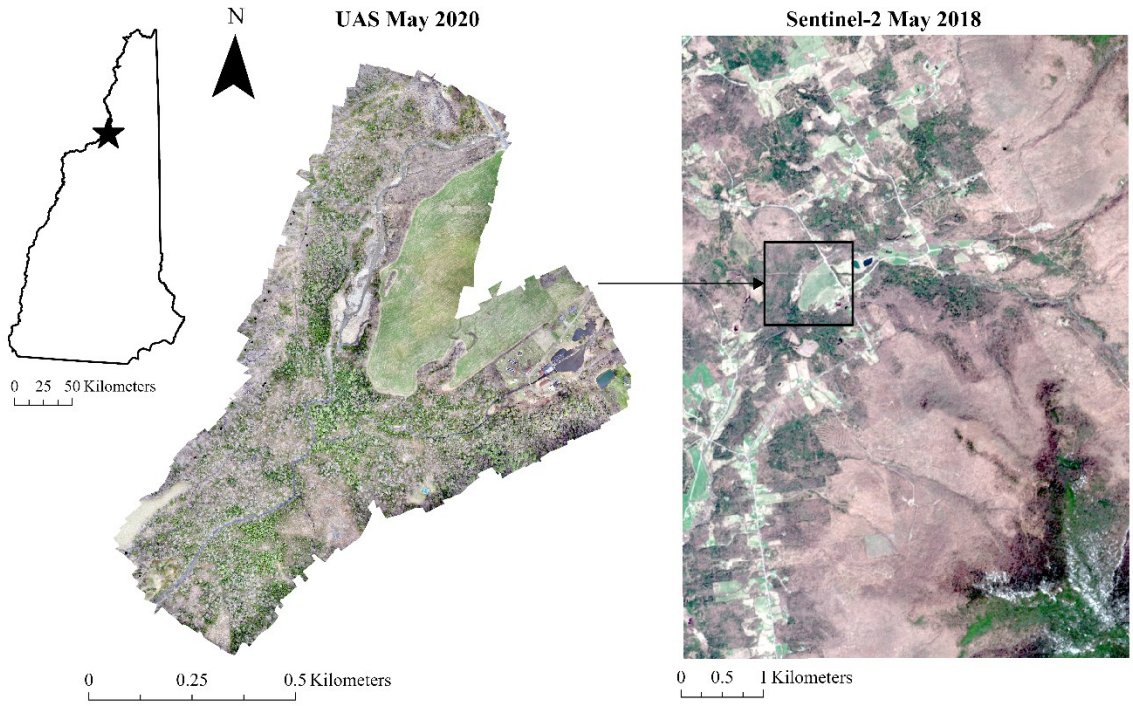

Figure 1: Study site at a regional scale represented with a Sentinel-2 image (May 2018), and local scale represented with UAS imagery (May 2020).

2.3 Focus Species

The invasive plant species *Fallopia japonica* (Japanese Knotweed) is an herbaceous perennial native to the east Asian countries of Japan, North China, Taiwan, and Korea (Dorigo et al. 2012) (Figure 2-A). It was introduced to the United States in the late 1800's for ornamental and horticultural purposes and is typically found growing in highly disturbed edge habitats such as roadways and riparian areas (Wilson et al., 2017; Aguilera et al., 2010). The plant is highly adaptable, able to tolerate wet or dry soils and limited sunlight. Japanese knotweed grows quickly, up to 20 centimeters in a day, and once established will form dense thickets up to three meters tall, blocking sunlight from reaching understory vegetation (Cygan, 2018; Wilson et al., 2017). The plant exhibits clonal growth, reproducing asexually through woody rhizomes that root as deep as 3 meters and extend laterally as far as 12 meters. Rhizome fragments that are displaced because of poor management practices (mowing/cutting) or from storm events can

propagate and begin new colonies downstream (Cygan, 2018; Rouifed et al., 2011). Additionally, the plant restricts the growth of other vegetation through the secretion of chemicals (allelopathy) and smothering, as the woody stalks create thick mats on the forest floor during the growing season (Wilson et al., 2017) (Figure 2-B).

Figure 2: Japanese knotweed. (a) Early spring growth, (b) Winter woody stalks.

2.4 Riparian Delineation

To obtain the necessary training data to perform the satellite imagery classification, I had to first determine the boundary of the riparian area for this study. There is no standard method to delineate riparian areas, and the process is influenced by the best management practices recommended for the particular ecosystem service or function that is being studied (Huylenbroeck et al., 2020; Felton et al., 2019). In this study, I aimed to define riparian

boundaries for habitat and vegetation protection, and therefore referenced the variable-width riparian delineation methodology as described in the report entitled, "Connect the Coast: Linking Wildlife Across New Hampshire's Seacoast and Beyond" (Steckler and Brickner-Wood, 2019). All delineation processes were completed in an ArcGIS Pro map project (ESRI, Redlands, California). A 2019 National Agricultural Image Program (NAIP) image (Geospatial Data Gateway; United States Department of Agriculture (USDA), Natural Resources Conservation Service (NRCS), Farm Service Agency (FSA)) was used as a basemap for visualization purposes only and had no bearing on the delineation process. The GIS data layers: National Hydrography Dataset (NHD), National Wetland Inventory (NWI), and 1-meter LiDAR-Based Digital Elevation (DEM) were downloaded from the New Hampshire Geographically Referenced Analysis and Information Transfer System (NH GRANIT; Earth Systems Research Center, Institute for the Study of Earth, Oceans, and Space, University of New Hampshire, Durham, New Hampshire). All streams and rivers of the fourth order were selected from the NHD layer; and used to create a new layer. The new NHD layer and original NWI layer were combined into one shapefile using the Merge tool and extracted to the site boundary using the Clip tool (Figure 4-A). Next, the shapefile was converted to a raster using the Feature to Raster tool (Figure 4-B) and given a horizontal buffer of 100 meters to extend 50 meters from the left and right stream banks (Figure 4-C). Then, the following processes were used to create a vertical buffer. Elevation values from the DEM were extracted to the rasterized NHD/NWI layer using the Extract Values to Points tool. Next, the Euclidean Allocation tool was run to a maximum horizontal distance of 200 meters resulting in a raster where pixel values represent the elevation at the closest NHD/NWI pixel. Then, using the Map Algebra tool, the Euclidean Allocation raster was subtracted from the original DEM, resulting in elevations above the closest NHD/NWI

cells (Figure 4-D). All cells outside of the 200-meter buffer were classified as "No Data" and were not included. The Map Algebra tool was used again to mask out Euclidean Allocation raster cells that were greater than 5 meters above the NHD/NWI cells (Figure 4-E). The result is a variable-width riparian delineation consisting of a 5-meter vertical buffer and a horizontal buffer of 50 meters (Figure 4-F).

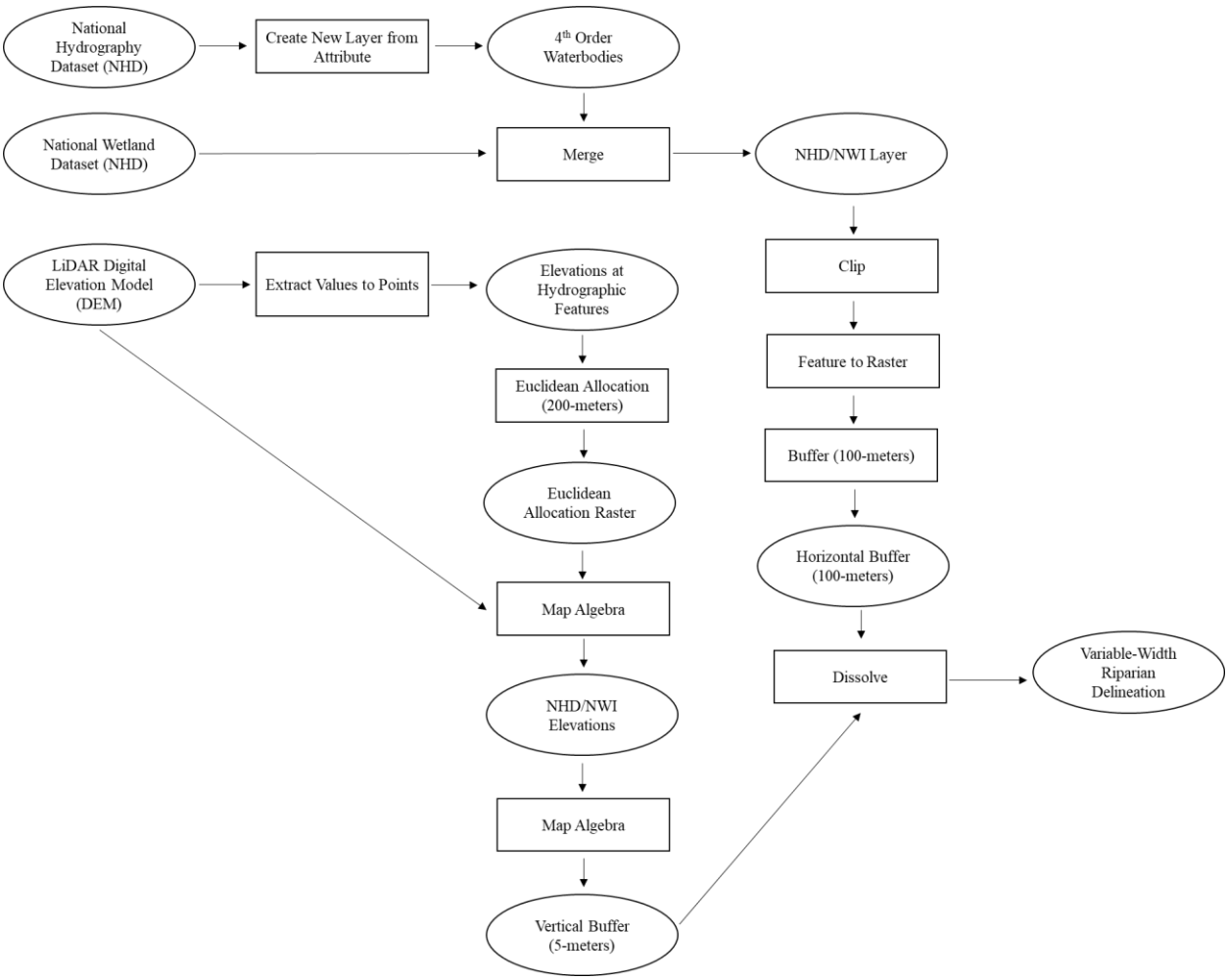

Figure 3: Riparian delineation workflow.

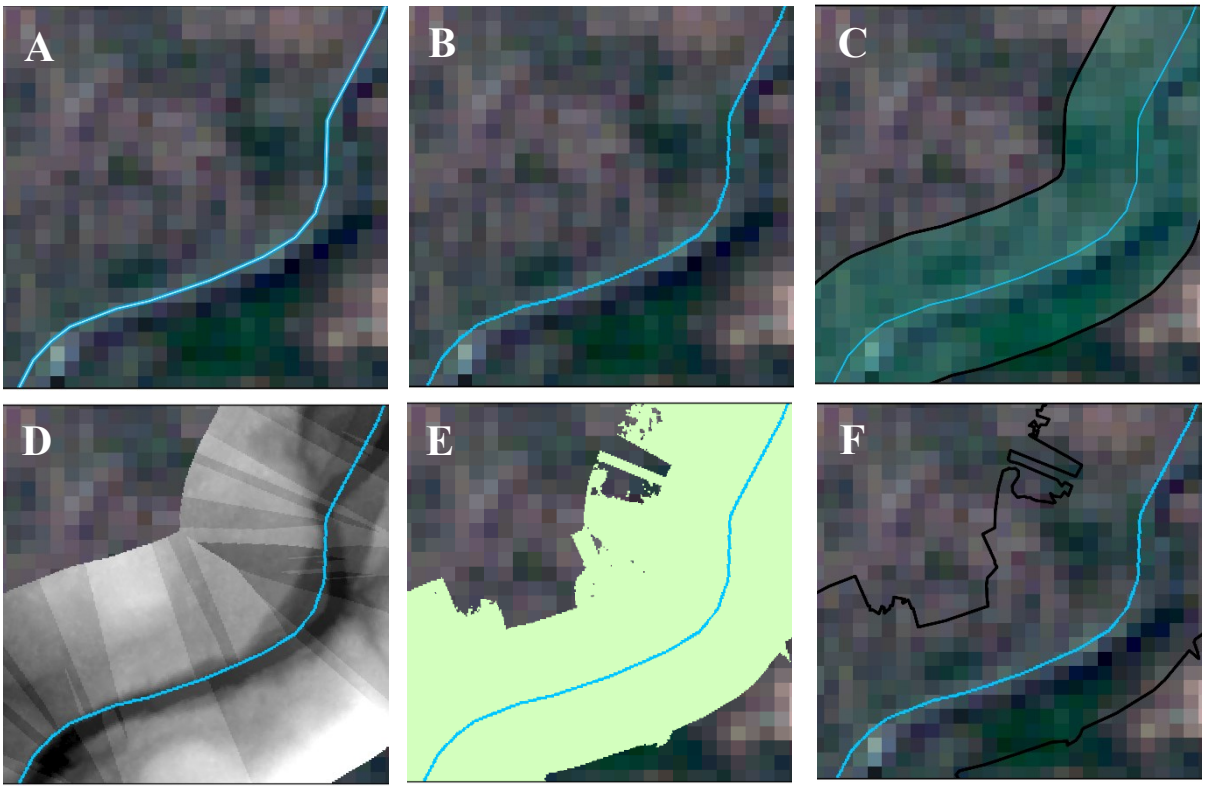

Figure 4: Riparian delineation process. (a) Vector stream, (b) Rasterized stream, (c) Rasterized stream with 100-meter horizontal buffer, (d) 200-meter horizontal buffer, (e) 5-meter vertical buffer, (f) Final riparian delineation with a 100-meter horizontal buffer and 5-meter vertical buffer.

2.5. Imagery Collection

For this study, I obtained Landsat 8 OLI and Sentinel-2 satellite imagery of early spring (leaf-off), summer (leaf-on), late summer, and autumn (fall senescence). Landsat 8 OLI imagery were downloaded from the United States Geological Survey (USGS) data portal, EarthExplorer. Sentinel-2 data were downloaded from the Copernicus Open Access Hub, a data portal operated by a collaboration between the European Union (EU) and the European Space Agency (ESA). The imagery was selected only if there was little/no cloud cover over the area of interest, which caused comparison imagery to be selected from various months and years. The selected Landsat

8 OLI imagery was from May 2018, June 2018, September 2017, and October 2020. The Sentinel-2 imagery was from May 2018, June 2018, August 2019, and October 2018.

For the UAS portion of the study, I flew two fixed-wing UAS: eBee Plus and eBee X (AgEagle Aerial Systems Inc. Wichita, Kansas). The eBee Plus was equipped with the Sensor Optimized for Drone Applications (S.O.D.A.), a 20-megapixel RGB sensor (AgEagle Aerial Systems Inc., Wichita, Kansas). The eBee X was equipped with the Aeria X, a 24-megapixel RGB sensor (AgEagle Aerial Systems Inc. Wichita, Kansas). Imagery was collected in leaf-off and leaf-on conditions during the spring, summer, and autumn throughout 2019, 2020, and 2021.

2.6 Reference Data

Reference data for the satellite classifications used the riparian delineation buffer to distinguish between riparian and non-riparian areas, and NAIP imagery (Geospatial Data Gateway; United States Department of Agriculture (USDA), Natural Resources Conservation Service (NRCS), Farm Service Agency (FSA)) from 2018 (leaf-off) and 2019 (leaf-on) to identify land cover in ArcGIS Pro (ESRI, Redlands, California). Satellite classifications included two primary classes: riparian and upland (Table 1). The primary classes were comprised of sub-categories (secondary classes) which describe the land cover: deciduous forest, coniferous forest, mixed forest, and grass/shrub. A total of 400 samples were collected, 200 for each primary class (riparian and upland). These samples were comprised of 50 samples for each secondary class (deciduous, conifer, mixed, grass/shrub), and were randomly split into groups of 25 for training and testing with the Subset Features tool in ArcGIS Pro.

The reference data for the UAS imagery were collected in the summer months of 2019 with a GPSMap64S (Garmin, Olathe, Kansas)**.** In total, 34 samples were identified in the study area, however only 21 were able to be used for processing due to canopy cover, patch size, and

deformations of orthomosaic edges. Like the satellite reference data, the samples were randomly divided into testing and training samples. Due to the uneven number of samples, 11 were used for training and 10 were used for testing.

Table 1: Satellite imagery classification scheme.

CLASSIFICATION SCHEME	
Primary	**Secondary**
Upland	Conifer
	Deciduous
	Grass/Shrub
	Mixed
Riparian	Riparian Conifer
	Riparian Deciduous
	Riparian Grass/Shrub
	Riparian Mixed

2.7 Satellite Image Processing and Classification

Prior to classifying the satellite imagery, I removed image bands that were extraneous to the goals of the study. From the 11-banded Landsat 8 OLI imagery, I removed the coastal aerosol, panchromatic, cirrus, and two thermal bands. From the 12-banded Sentinel-2 imagery, I removed the coastal aerosol, water vapor, and short-wave infrared cirrus bands. I also calculated three vegetation indices for each image in ERDAS IMAGINE (Hexagon AB, Stockholm, Sweden): Moisture Stress Index (MSI), Normalized Difference Vegetation Index (NDVI) and Normalized Difference Water Index (NDWI). MSI measures the leaf water content and is calculated using the formula MSI = Short Wave Infrared (SWIR) / Near Infrared (NIR) (Mahato et al., 2021). NDVI measures vegetation health and is calculated with the equation NDVI = (NIR – Red) / (NIR + Red)(Jensen, 2016). NDWI measures wetness with the calculation NDWI = (Green - NIR) / (Green + NIR) (Barron et al, 2012). Once the index layers were created, they

were added to the respective images through the layer stacking function in the software, resulting in 9-banded Landsat 8 OLI images and 13-banded Sentinel-2 images.

I performed a supervised object-based image analysis (OBIA) classification on each of the single-date satellite images using the eCognition software (Trimble, Westminster, Colorado). The images were segmented using the multiresolution segmentation (MRS) technique. This technique creates segments based off three major parameters: scale, shape, and compactness. To obtain optimal parameters for the final segmentation, I ran multiple iterations of the segmentation process and generated a report of the object statistics with each iteration to determine object size and band importance. Parameters that yielded image objects > 10 cells were rejected to avoid over-segmentation. The optimal parameters varied between the satellites and between seasons (Table 2). Band importance also varied for each image, and the top three were given a higher weight than the other bands. Once segmented, the image objects were classified using the Random Forests classifier (Breiman, 2001). I set the classifier to a maximum of 500 trees and utilized various object variables: means and standard deviations for each image band and vegetation index and brightness. There was a total of 19 object variables for the Landsat 8 OLI images, and 27 for the Sentinel-2 images.

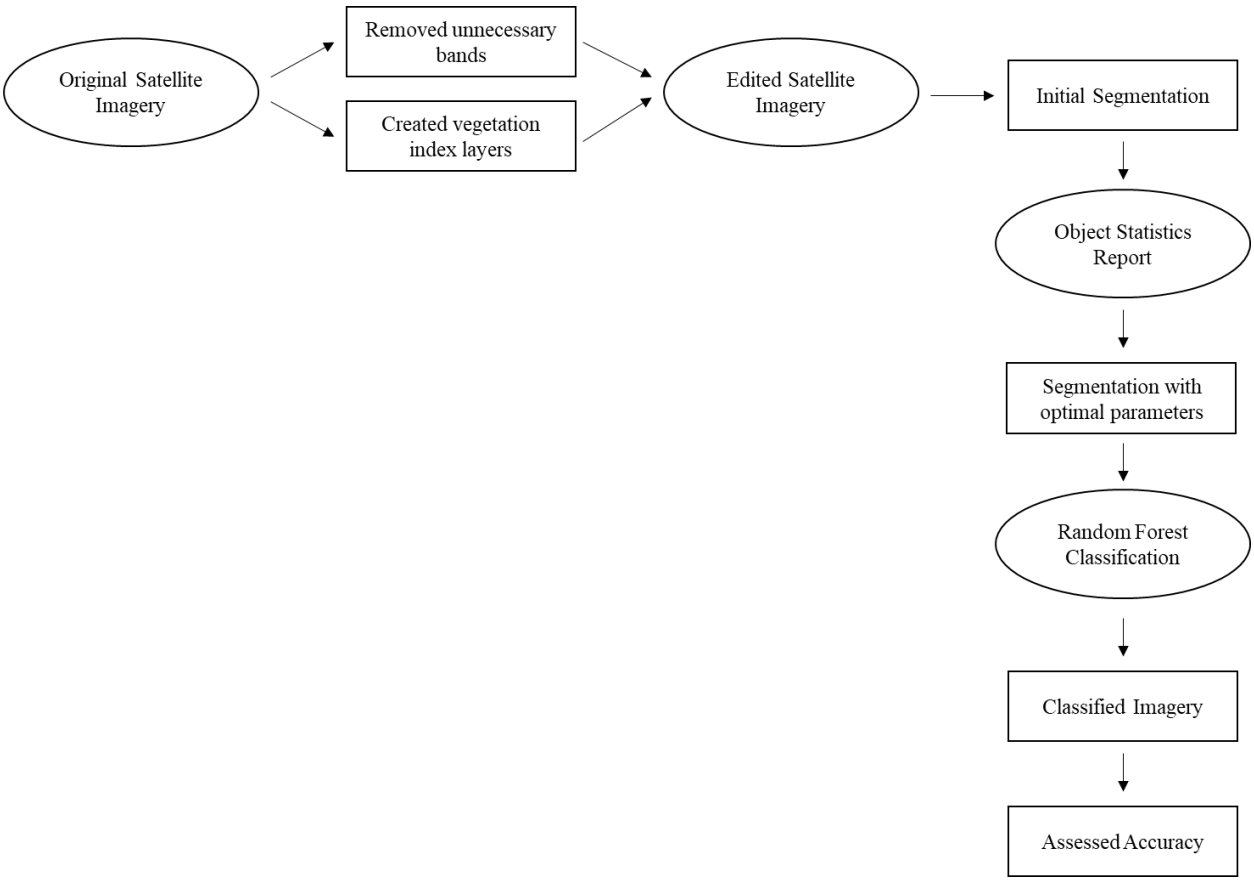

Figure 5: Satellite imagery classification workflow.

Table 2: Classification parameters for the single-date satellite classifications.

Satellite	Month	Scale	Shape	Compactness
Landsat 8	May	60	0.1	0.5
Landsat 8	June	60	0.1	0.4
Landsat 8	September	40	0.1	0.9
Landsat 8	October	50	0.1	0.7
Sentinel	May	60	0.2	0.7
Sentinel	June	60	0.2	0.7
Landsat 8	August	60	0.2	0.7
Sentinel	October	50	0.5	0.5

Once the single-date satellite images were classified, I extracted the three most important bands from each of the Landsat 8 OLI and Sentinel-2 images in ERDAS IMAGINE (Hexagon AB, Stockholm, Sweden). The top three bands for each satellite were then combined through the layer stack function to create three multi-date combinations: early spring + late summer, early spring + fall, early spring + late summer + fall (Table 3, Table 4). The multi-date combinations were then classified in the same manner as the single-date images. For the Landsat 8 OLI multi-date image, the optimal parameters were a scale of 50, shape of 0.1, and compactness of 0.5. The optimal parameters for the Sentinel-2 multi-date image were a scale of 60, shape of 0.2, and compactness of 0.7.

Table 3: Band importance of the **Landsat 8 OLI** multi-date image.

Month & Band	Importance
May- (Short-wave Infrared 2)	1
May- (Short-wave Infrared 1)	0.97
October- (Short-wave Infrared 2)	0.84
September- (Short-wave Infrared 1)	0.83
May- (Green)	0.74
September- (Green)	0.72
June- (Short-wave Infrared 1)	0.41
Sept- (Short-wave Infrared 2)	0.37
June- (Short-wave Infrared 1)	0.32
October- (Red)	0.27
June- (Red)	0.23
October- (Short-wave Infrared 1)	0.15

Table 4: Band importance of the **Sentinel-2** multi-date image.

Month & Band	Importance
August- (Short-wave Infrared 2)	1
August- (Short-wave Infrared 1)	0.97
May- (Short-wave Infrared 2)	0.84
May- (Vegetation Red Edge 1)	0.83
May- (Short-wave Infrared 1)	0.74
August- (Short-wave Infrared 2)	0.72
June-(Blue)	0.41
June- (Red)	0.37
June- (Short-wave Infrared 1)	0.32
October- (Short-wave Infrared 2)	0.27
October- (Blue)	0.23
October- (Short-wave Infrared 1)	0.15

2.8 UAS Image Processing and Classification

After each flight, the UAS log and imagery were uploaded to the eMotion software (AgEagle Aerial Systems Inc., Wichita, Kansas) so that the imagery could be Post-Process Kinematic (PPK) corrected using data from the VTD7 Continuously Operating Reference Station (CORS) (National Geodetic Survey, 2019-2021). Then, to create a georeferenced orthomosaic, all imagery was processed using the Agisoft Metashape software (Agisoft LLC, Saint Petersburg, Russia). Each orthomosaic was processed to be at a spatial resolution of between 2 and 3 centimeters.

I then performed a supervised, object-based image analysis (OBIA) classification on the UAS imagery using the Random Forest Algorithm in the eCognition software (Trimble, Westminster, Colorado) (Breiman, 2001). The images were segmented using the MRS technique, and the parameters were set to a scale of 500, shape of 0.1, and compactness of 0.5. I elected to use the Random Forest classifier to classify the UAS imagery due to the robustness of the classifier to small training sets. The Random Forest algorithm parameters were set to a maximum

of 500 trees and utilized the object variables: means and standard deviations for each band, and the brightness.

2.9 Accuracy Assessment

To assess the accuracy of the satellite and UAS classifications, I created an error matrix for each of the 22 thematic maps. An error matrix is a way to measure of the agreement and disagreement between the reference data and the classified data and is created by comparing the testing samples of the reference data to the class it was assigned in the thematic map (Congalton and Green, 2019). The error matrix is comprised of rows which represent the classified (i.e., the results of classifying the imagery data and columns which represent the reference data.

From the error matrices, I generated three accuracy statistics: overall (OA), user's (UA), and producer's (PA) (Story and Congalton, 1986). The accuracy of the entire map is represented by the OA. It is calculated by summing the major diagonal values and dividing the result by the total number of samples (Congalton and Green, 2019). The UA represents the commission error, or the probability that the test sample was included in the incorrect map class; it is calculated by dividing the major diagonal value for each map class by the row total for the specific class. The PA represents the omission error, or the probability that the test sample was excluded from the correct map class; it is calculated by dividing the major diagonal value for each map class by the column total for the specific class (Congalton and Green, 2019; Story and Congalton, 1986).

2.10 Results

The single-date satellite primary classification that achieved the highest overall accuracies were the May and October Sentinel-2 images at 59% (Table 5, Table 6, Table 7, Figure 6, Figure 7). These classifications also obtained the same user's and producer's accuracies (Table 6, Table 7). The primary classifications of the satellite images scored higher accuracies than the secondary classifications (Table 5, Table 8). The May Sentinel-2 image also achieved the highest accuracy of all secondary classifications at 52% and outperformed the secondary classification of the October imagery (Table 9, Table 10).

Table 5: Comparison of overall (OA), user's (UA), and producer's (PA) accuracies for the single-date primary classifications of the satellite imagery. Highlighted rows have the best overall accuracy.

Month	Status	Satellite	OA	UA	PA
May	Leaf Off	Landsat 8	52%	52%	46%
May	Leaf Off	Sentinel	59%	58%	64%
June	Leaf On	Landsat 8	52%	52%	48%
June	Leaf On	Sentinel	55%	56%	45%
Early September	Leaf On	Landsat 8	54%	53%	60%
Late August	Leaf On	Sentinel	50%	49%	43%
October	Fall Senescence	Landsat 8	56%	56%	60%
October	Fall Senescence	Sentinel	59%	58%	64%

Table 6: Error matrix of the primary classification of the May Sentinel-2 imagery.

MAP DATA	REFERENCE DATA				
	Primary Classification	Riparian	Upland	TOTAL	*User's Accuracy*
	Riparian	53	47	100	53%
	Upland	35	65	100	35%
	TOTAL	88	112	200	*Overall Accuracy*
Prodcuer's Accuracy		60%	42%		59%

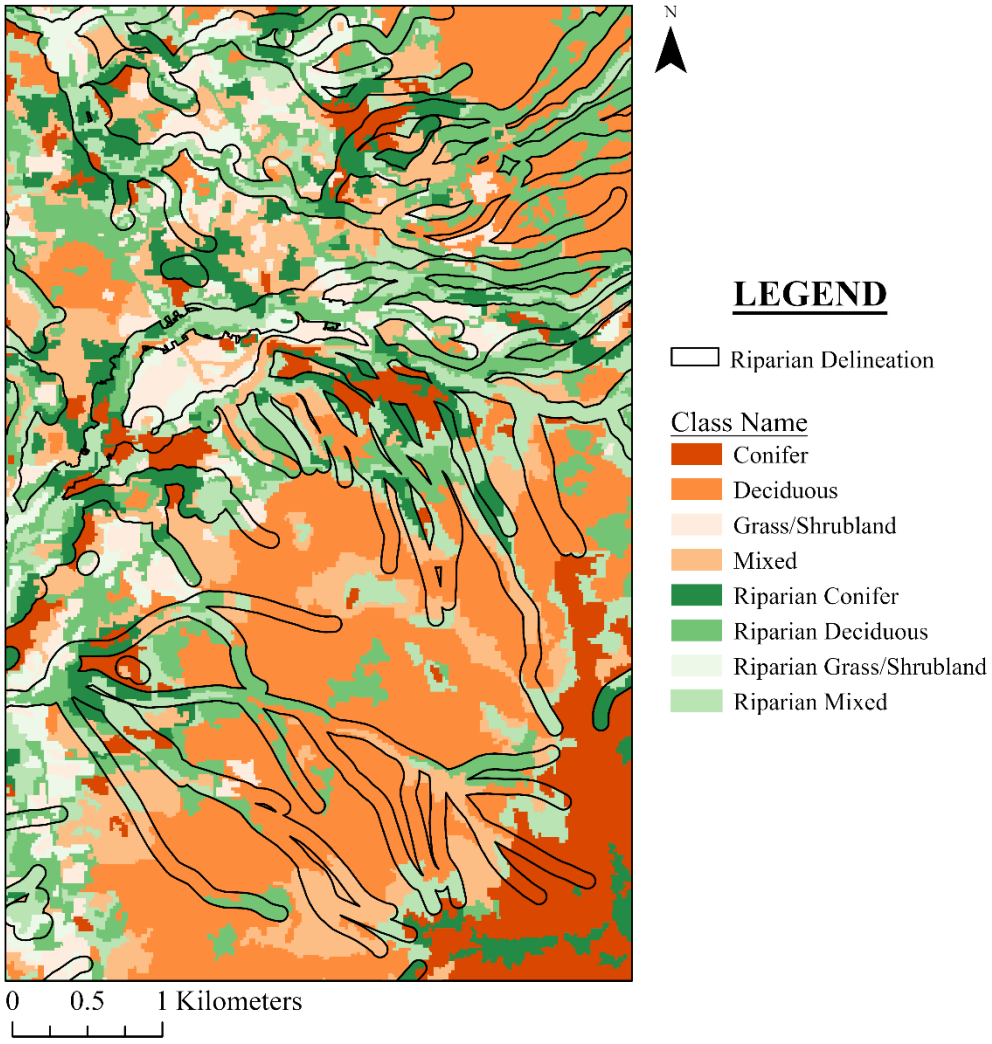

Figure 6: Classification map of the May Sentinel-2 image.

Table 7: Error matrix of the primary classification of the October Sentinel-2 imagery.

MAP DATA	REFERENCE DATA				
	Primary Classification	Riparian	Upland	TOTAL	*User's Accuracy*
	Riparian	64	46	110	58%
	Upland	36	54	90	40%
	TOTAL	100	100	200	*Overall Accuracy*
Prodcuer's Accuracy		64%	46%		59%

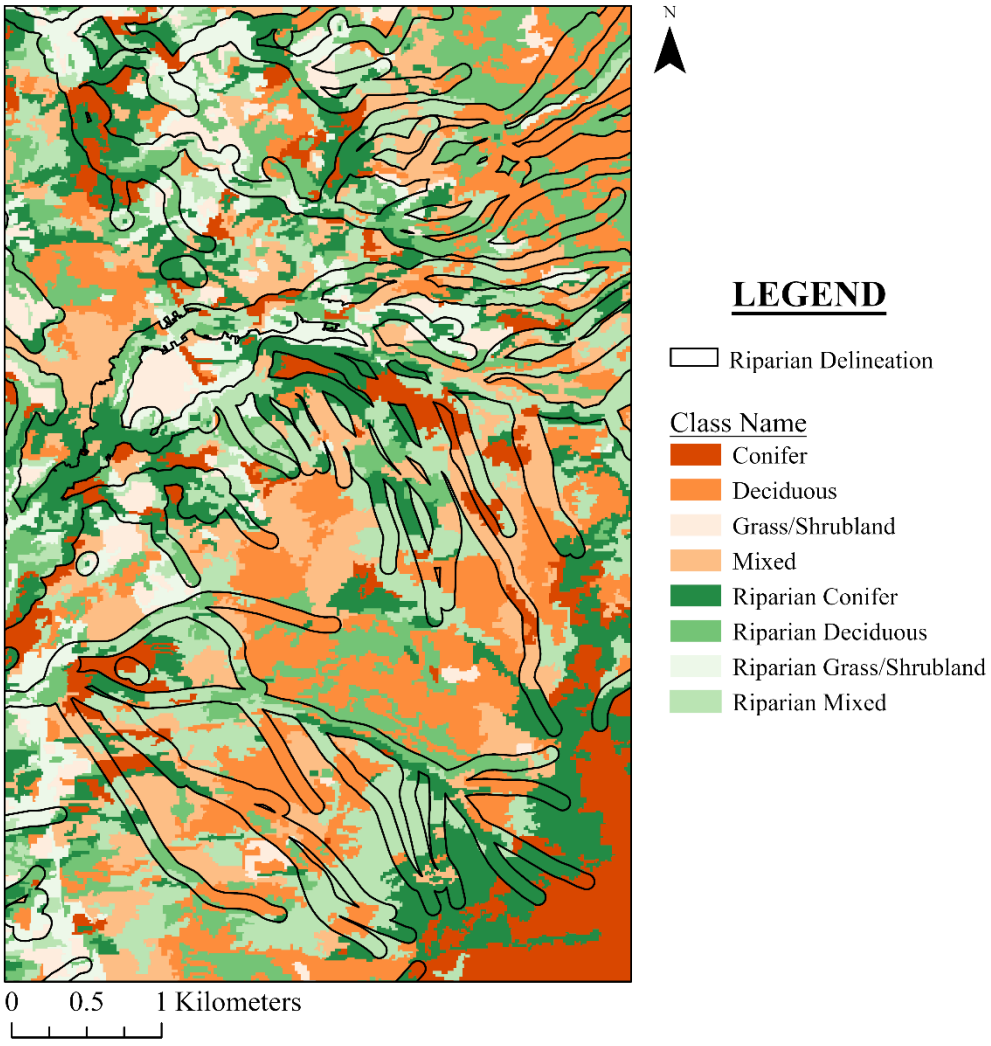

Figure 7: Classification map of the October Sentinel-2 image.

Table 8: Comparison of the overall (OA) accuracies for the single-date secondary classifications of the satellite imagery. Highlighted rows have the best overall accuracy.

Month	Status	Satellite	OA
May	Leaf Off	Landsat 8	45%
May	Leaf Off	Sentinel	52%
June	Leaf On	Landsat 8	35%
June	Leaf On	Sentinel	40%
Early September	Leaf On	Landsat 8	38%
Late August	Leaf On	Sentinel	38%
October	Senescence	Landsat 8	39%
October	Senescence	Sentinel	38%

Table 9: Error matrix of the secondary classification of the May Sentinel-2 imagery.

			REFERENCE DATA									
		Primary Classification	Upland				Riparian				TOTAL	*User's Accuracy*
		Secondary Classification	Conifer	Deciduous	Grass/Shrub	Mixed	Conifer	Deciduous	Grass/Shrub	Mixed		
MAP DATA	Upland	Conifer	17	0	0	0	11	0	0	0	28	61%
		Deciduous	0	17	1	1	0	9	0	0	28	61%
		Grass/Shrub	0	1	15	0	0	2	16	0	34	44%
		Mixed	1	1	0	11	0	3	0	6	22	50%
	Riparian	Conifer	6	0	0	0	13	0	0	2	21	39%
		Deciduous	0	5	2	3	0	9	2	2	23	39%
		Grass/Shrub	0	0	7	0	0	0	7	0	14	50%
		Mixed	1	1	0	10	1	2	0	15	30	50%
		TOTAL	25	25	25	25	25	25	25	25	200	*Overall Accuracy*
Producer's Accuracy			68%	68%	60%	44%	52%	36%	28%	60%		52%

Table 10: Error matrix of the secondary classification of the October Sentinel-2 imagery.

			REFERENCE DATA									
		Primary Classification	Upland				Riparian				TOTAL	*User's Accuracy*
		Secondary Classification	Conifer	Deciduous	Grass/Shrub	Mixed	Conifer	Deciduous	Grass/Shrub	Mixed		
MAP DATA	Upland	Conifer	10	0	0	2	9	0	0	0	21	48%
		Deciduous	0	12	2	2	0	6	0	5	27	44%
		Grass/Shrub	0	0	9	0	0	1	10	0	20	45%
		Mixed	4	4	0	9	2	0	0	3	22	41%
	Riparian	Conifer	11	0	0	3	10	1	1	4	30	38%
		Deciduous	0	5	0	1	0	8	3	4	21	38%
		Grass/Shrub	0	0	13	0	0	2	11	2	28	39%
		Mixed	0	4	1	8	4	7	0	7	31	23%
		TOTAL	25	25	25	25	25	25	25	25	200	*Overall Accuracy*
Producer's Accuracy			40%	48%	36%	36%	40%	32%	44%	28%		38%

Similar to the single date classifications, the multi-date satellite primary classifications outperformed the secondary classifications (Table 11, Table 13). The Landsat 8 OLI (spring + summer + autumn) combination achieved the highest overall accuracy at 62% (Table 12, Figure 8). The multi-date secondary classifications all reported similar overall accuracies ranging from 42-46% (Table 13).

Table 11: Comparison of the overall (OA) accuracies for the multi-date primary classifications of the satellite imagery. Highlighted rows have the best overall accuracy.

Satellite	Month Combination	OA
Landsat 8	May + October	46%
Sentinel	May + October	53%
Landsat 8	May + September	59%
Sentinel	May + August	54%
Landsat 8	May + September + October	62%
Sentinel	May + August + October	46%

Table 12: Error matrix of the primary classification of the Landsat 8 multi-date imagery.

MAP DATA	REFERENCE DATA				
	Primary Classification	Riparian	Upland	TOTAL	*User's Accuracy*
	Riparian	62	38	100	62%
	Upland	38	62	100	38%
	TOTAL	100	100	200	*Overall Accuracy*
Prodcuer's Accuracy		62%	38%		62%

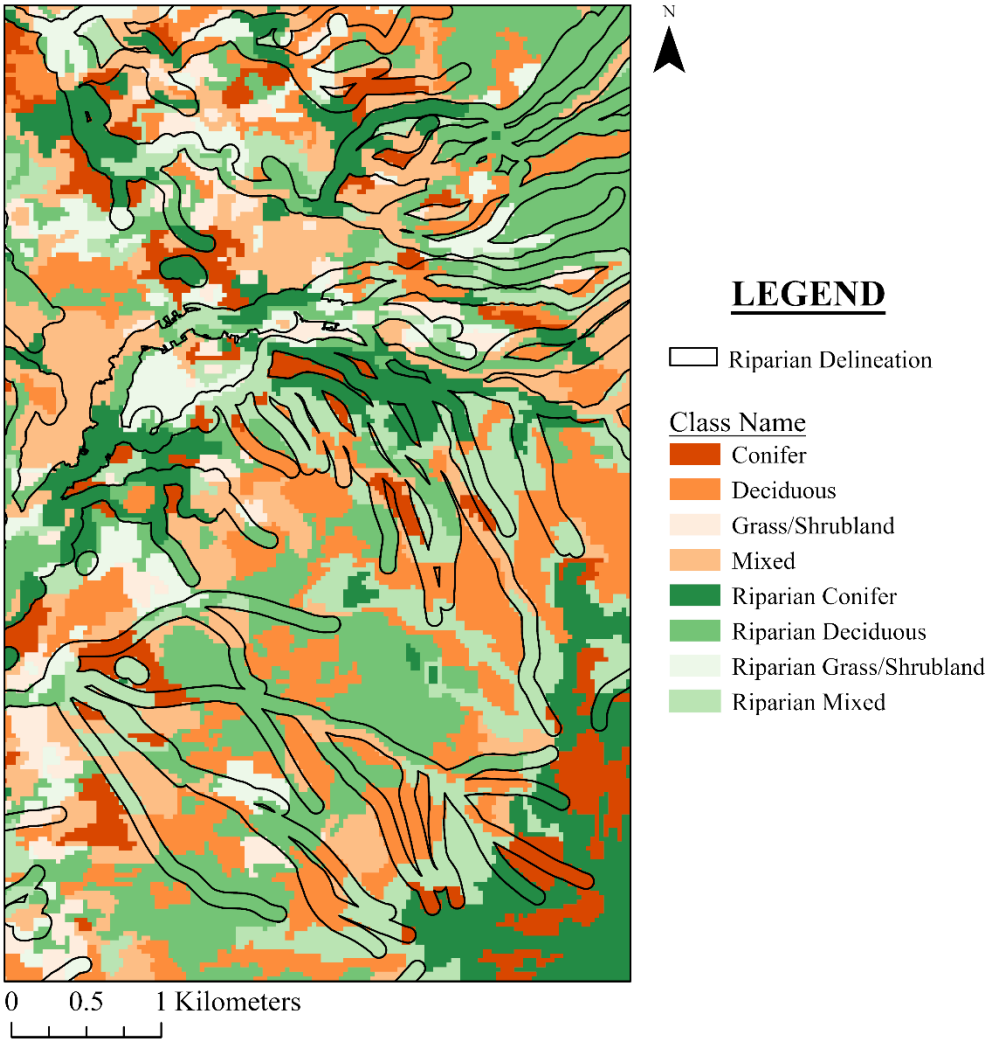

Figure 8: Classification map of the Landsat 8 OLI (spring + summer + autumn) multi-date image.

Table 13: Comparison of the overall (OA) accuracies for the multi-date secondary classifications of the satellite imagery.

Satellite	Month Combination	OA
Landsat 8	May + October	44%
Sentinel	May + October	45%
Landsat 8	May + September	46%
Sentinel	May + August	44%
Landsat 8	May + September + October	42%
Sentinel	May + August + October	45%

The most accurate classifications of the unmanned aerial system (UAS) imagery were October 2019 and 2020 (Table 14, Table 15, Table 16, Figure 9, Figure 10). The October 2019 classification surpassed the October 2020 classification in terms of user's accuracy, but the October 2020 achieved a higher producer's accuracy (Table 14). The second highest overall accuracy was obtained by the September 2019 classification, outperforming the September 2020 classification (Table 14). The classifications with the poorest overall accuracies were June 2019, September 2020, and May 2021 at 55% (Table 14).

Table 14: Comparison of overall (OA), user's (UA), and producer's (PA) accuracies for the invasive species classifications of the UAS imagery.

Month	Year	Season	Status	OA	UA	PA
June	2019	Early Summer	Leaf On	55%	70%	70%
September	2019	Early Autumn	Early Fall	65%	70%	64%
October	2019	Autumn	Fall Senescence	70%	70%	70%
May	2020	Early Spring	Leaf Off	60%	80%	57%
July	2020	Summer	Leaf On	60%	60%	60%
September	2020	Early Autumn	Early Fall	55%	50%	56%
October	2020	Autumn	Fall Senescence	70%	60%	75%
May	2021	Spring	Leaf Off	55%	40%	57%

Table 15: Error matrix of the October 2019 UAS imagery.

MAP DATA	REFERENCE DATA				
	Primary Classification	Invasive	Not Invasive	TOTAL	*User's Accuracy*
	Invasive	7	3	10	70%
	Not Invasive	3	7	10	30%
	TOTAL	10	10	20	*Overall Accuracy*
	Producer's Accuracy	70%	30%		70%

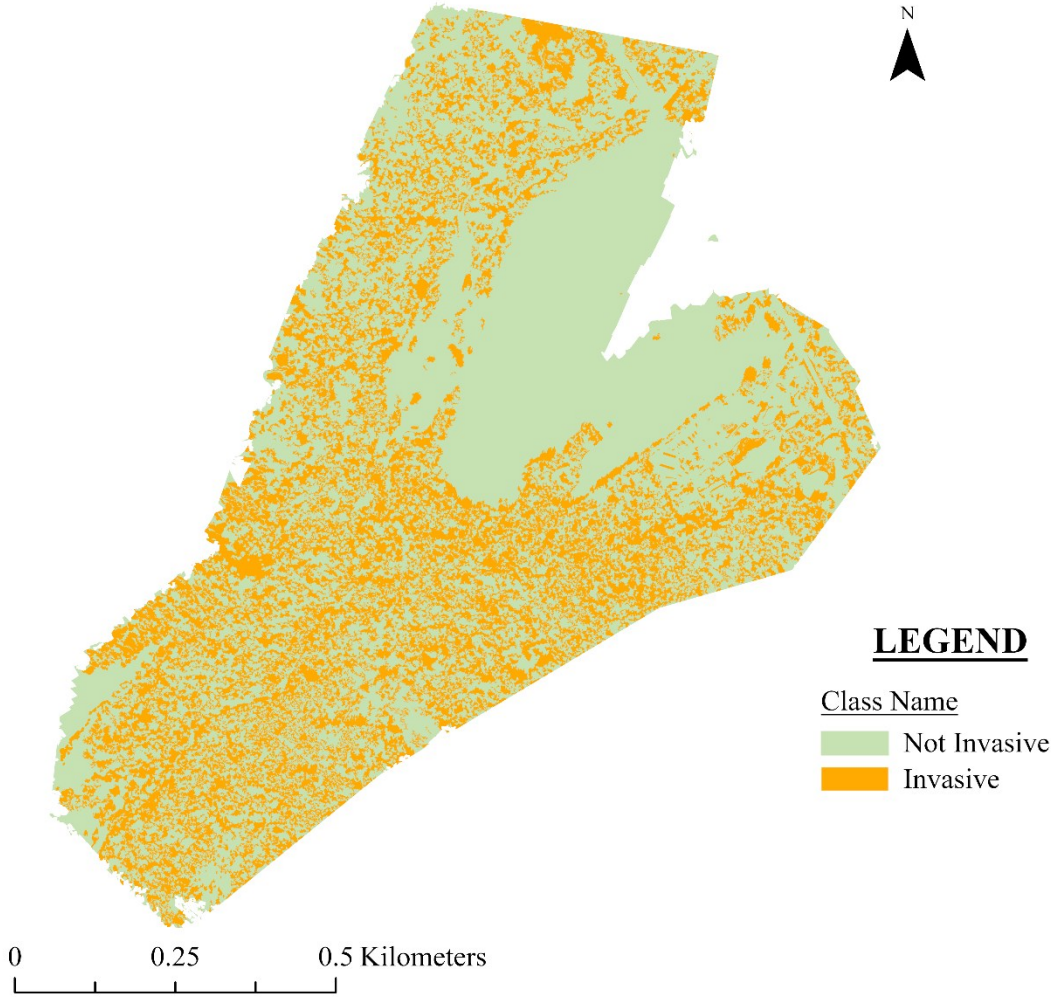

Figure 9: Classification map of the October 2019 UAS imagery.

Table 16: Error matrix of the October 2020 UAS imagery.

MAP DATA	REFERENCE DATA				
	Primary Classification	Invasive	Not Invasive	TOTAL	*User's Accuracy*
	Invasive	6	4	10	60%
	Not Invasive	2	8	10	20%
	TOTAL	8	12	20	*Overall Accuracy*
	Producer's Accuracy	75%	33%		70%

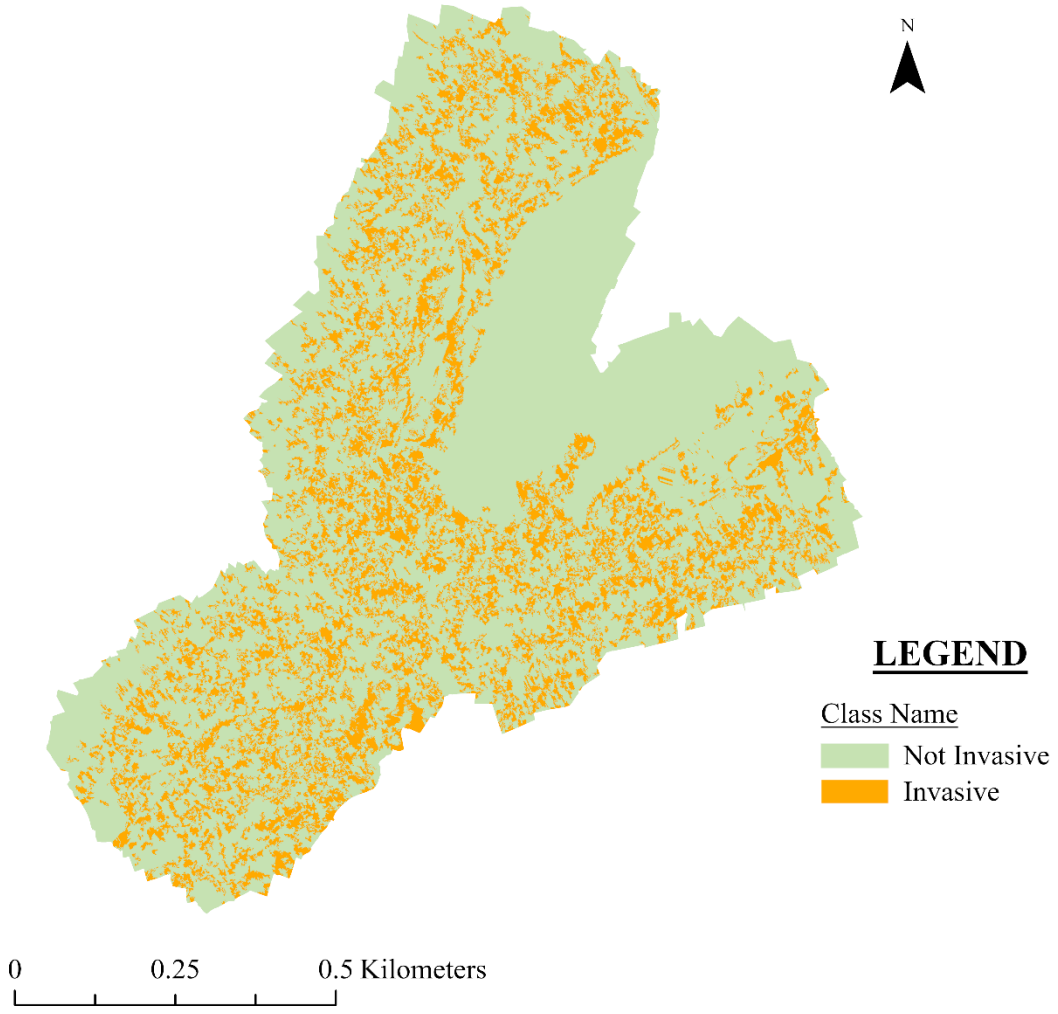

Figure 10: Classification map of the October 2020 UAS imagery.

2.11 Discussion

The primary classifications of the satellite imagery generated thematic maps that were up to 62% accurate. As suggested by *Congalton et al., 2002* to improve the accuracy of moderate resolution imagery, these classifications sampled riparian and non-riparian vegetation separately. Although these results do surpass those from the *Congalton et al., 2002* study which did not utilize these methods, they are not comparable to the studies conducted by *Baker et al., 2006* and *Villarreal et al., 2012* which obtained accuracies up to 86%, and 91%, respectively. However, these results still indicate that this sampling technique can improve the overall accuracies of thematic maps with moderate resolution imagery. In addition to testing sampling methods, I also utilized vegetation indices to potentially enhance the differences between riparian and non-riparian vegetation as presented in by the *Barron et al.* (2012) study. The multi-date satellite images were comprised of the most important bands as per the object statistics generated by the classification algorithm; and did not indicate that the vegetation indices were highly important.

The Sentinel-2 single-date primary classifications typically outperformed the respective Landsat 8 OLI classifications in terms of overall accuracy, while the opposite is true for the multi-date primary classifications. These mixed results do not indicate that either moderate resolution satellite (Landsat 8 OLI, 30 m; Sentinel-2, 10 m) is superior when mapping riparian areas. Both satellites obtained poor accuracies for the single and multi-date secondary classifications. These results reinforce the notion that moderate resolution imagery is limited when mapping riparian vegetation, and that high resolution imagery are required for higher accuracies (Huylenbroeck et al., 2020; Yang, 2007; Goetz, 2006; Congalton et al., 2002).

The best single-date primary classification accuracy achieved by the Landsat 8 OLI imagery was the October (fall senescence) image at 56%, and October (fall senescence) and May

(leaf off) for the Sentinel-2 imagery at 59%. The lowest accuracies were obtained with the May (leaf off) Landsat 8 OLI and August (leaf on) Sentinel-2 imagery. These results indicate that differences between riparian and non-riparian vegetation may be maximized during fall senescence and could be related to water availability (Barron et al. 2012).

The UAS invasive species classifications generated thematic maps with overall accuracies ranging from 55 to 70%, which are comparable to the results obtained by *Michez et al.* (2016) (OA = 58-69%). The most accurate classifications were the October 2019 and 2020 classifications; however, the October 2019 classification has a higher user's accuracy than the October 2020 classification, but a lower producer's accuracy. The user's accuracy represents commission error (i.e., false positive) while the producer's accuracy represents omission errors (i.e., false negative). While predicting the location of invasive species, it is more important to avoid false negatives than false positive, because it is better to mislabel an area as invaded than miss a patch that could become a colony (Uden et al., 2015). Therefore, the October 2020 classification is superior to the October 2019 classification. In comparison to the high accuracies achieved by these dates, the June 2019 and May 2021 classifications produced the poorest overall accuracies at 55%. The phenology of Japanese knotweed is most prominent during late summer when it flowers and fall senescence when the flowers and stalks turn a rusty orange, brown color (Dorigo et al., 2012). These results suggest that phenology and timing of imagery acquisition play an importance role in the detection of invasive species (Müllerová et al., 2017). Although the UAS classifications generated positive results, the sample size was extremely limited, which reduces the significance of the study. The results of the UAS classifications serve as an observation, and a larger sample size is required.

There were two major limitations encountered by the study. Firstly, the data collected for the satellite imagery classifications were from different months and years; primarily due to clouds covering the area of interest. It is possible that land cover changes occurred between compared imagery and skewed the classification results. Secondly, the UAS classifications were generated from a small sample size. The issue was further compounded because one third of the samples were not visible in the UAS imagery due to canopy cover, patch size, and deformations of the orthomosaics. The limited number of samples were insufficient to garner the results as significant.

Future studies could expand upon the methods used in this study to create the riparian delineation and the satellite imagery sampling method. The variable width riparian delineation method could be improved through the use of additional variables, such as soil type and flood plain extents. The study found evidence that the riparian and upland sampling technique proposed by *Congalton et al., 2002* improved the use of moderate resolution imagery for the mapping of riparian areas, and future studies could investigate the use of this sampling method to other moderate resolution satellite imagery.

2.12 Conclusion

This was a proof-of-concept study that aimed to firstly investigate the use of moderate resolution satellite imagery to map riparian areas and secondly, to test the feasibility of UAS imagery to map the invasive plant Japanese knotweed. I have demonstrated that riparian areas can be delineated with modest success using moderate resolution satellite imagery and observed that UAS can be used to detect invasive plants in riparian habitat. Although some satellite classifications outperformed the others, neither Landsat 8 OLI nor Sentinel-2 were necessarily better than the other despite a difference in spatial resolution. It is possible to use moderate

resolution satellite imagery to map riparian habitat if due consideration is given to the sampling methods and when imagery is captured. Additionally, the study observed that UAS imagery have the potential to classify Japanese knotweed in riparian areas accurately if the data is collected during prime phenological windows, especially in autumn.

REFERENCES

Allen, J. M., Leininger, T. J., Hurd, J. D., Civco, D. L., Gelfand, A. E., & Silander, J. A. (2013). Socioeconomics drive woody invasive plant richness in New England, USA through forest fragmentation. Landscape Ecology, 28(9), 1671–1686.

Baker, C., Lawrence, R., Montagne, C., & Patten, D. (2006). Mapping wetlands and riparian areas using Landsat ETM+ imagery and decision-tree-based models. Wetlands, 26(2), 465–474.

Barron, O. V., Emelyanova, I., Van Niel, T. G., Pollock, D., & Hodgson, G. (2014). Mapping groundwater-dependent ecosystems using remote sensing measures of vegetation and moisture dynamics. Hydrological Processes, 28(2), 372–385.

Bradley, B. A., Blumenthal, D. M., Wilcove, D. S., & Ziska, L. H. (2010). Predicting plant invasions in an era of global change. Trends in Ecology & Evolution, 25(5), 310–318.

Breiman, L. (2001) Random Forests. Machine Learning, 45, 5-32.

Cánovas-García, F., & Alonso-Sarría, F. (2015). A local approach to optimize the scale parameter in multiresolution segmentation for multispectral imagery. Geocarto International, 30(8), 937–961.

Congalton, R. G. (1991). A review of assessing the accuracy of classifications of remotely sensed data. Remote Sensing of Environment, 37(1), 35–46.

Congalton, R. G., Birch, K., Jones, R., & Schriever, J. (2002). Evaluating remotely sensed techniques for mapping riparian vegetation. Computers and Electronics in Agriculture, 37(1–3), 113–126.

Congalton, R., Green, K., 2019. Assessing the Accuracy of Remotely Sensed Data: Principles and Practices, 3rd ed. CRC Press, Boca Raton, FL.

Crall, A. W., Newman, G. J., Jarnevich, C. S., Stohlgren, T. J., Waller, D. M., & Graham, J. (2010). Improving and integrating data on invasive species collected by citizen scientists. Biological Invasions, 12(10), 3419–3428.

de Sosa, L. L., Glanville, H. C., Marshall, M. R., Abood, S. A., Williams, A. P., & Jones, D. L. (2018). Delineating and mapping riparian areas for ecosystem service assessment. Ecohydrology, 11(2), 1–1.

Dorigo, W., Lucieer, A., Podobnikar, T., & Čarni, A. (2012). Mapping invasive Fallopia japonica by combined spectral, spatial, and temporal analysis of digital orthophotos. International Journal of Applied Earth Observation and Geoinformation, 19, 185–195.

Ehrenfeld, J. G. (2010). Ecosystem Consequences of Biological Invasions. Annual Review of Ecology, Evolution, and Systematics, 41, 59–80.

Executive Order 13112, 1999. Executive Order 13112 of February 3, 1999, Federal Register. United States.

Felton, B. R., O'Neil, G. L., Robertson, M.-M., Fitch, G. M., & Goodall, J. L. (2019). Using Random Forest Classification and Nationally Available Geospatial Data to Screen for Wetlands over Large Geographic Regions. Water, 11(6), Article 6.

Finch, D. M., Butler, J. L., Runyon, J. B., Fettig, C. J., Kilkenny, F. F., Jose, S., Frankel, S. J., Cushman, S. A., Cobb, R. C., Dukes, J. S., Hicke, J. A., & Amelon, S. K. (2021). Effects of Climate Change on Invasive Species. In T. M. Poland, T. Patel-Weynand, D. M. Finch, C. F. Miniat, D. C. Hayes, & V. M. Lopez (Eds.), *Invasive Species in Forests and Rangelands of the United States: A Comprehensive Science Synthesis for the United States Forest Sector* (pp. 57–83). Springer International Publishing.

Fu, B., & Burgher, I. (2015). Riparian vegetation NDVI dynamics and its relationship with climate, surface water and groundwater. Journal of Arid Environments, 113, 59–68.

Gao, Y., & Mas, J. F. (2008). A comparison of the performance of pixel-based and object-based classifications over images with various spatial resolutions. Online journal of earth sciences, 2(1), 27-35.

Goetz, S. J. (2006). Remote Sensing of Riparian Buffers: Past Progress and Future Prospects1. JAWRA Journal of the American Water Resources Association, 42(1), 133–143.

González del Tánago, M., & García de Jalón, D. (2006). Attributes for assessing the environmental quality of riparian zones. Limnética, 25(1–2), 389–402.

Hayes, S. J., & Holzmueller, E. J. (2012). Relationship between Invasive Plant Species and Forest Fauna in Eastern North America. Forests, 3(3), Article 3.

Hejda, M., Pyšek, P., & Jarošík, V. (2009). Impact of invasive plants on the species richness, diversity and composition of invaded communities. Journal of Ecology, 97(3), 393–403.

Hess, M. C. M., Mesléard, F., & Buisson, E. (2019). Priority effects: Emerging principles for invasive plant species management. Ecological Engineering, 127, 48–57.

Hossain, M. D., & Chen, D. (2019). Segmentation for Object-Based Image Analysis (OBIA): A review of algorithms and challenges from remote sensing perspective. ISPRS Journal of Photogrammetry and Remote Sensing, 150, 115–134.

Huang, C., & Asner, G. P. (2009). Applications of Remote Sensing to Alien Invasive Plant Studies. Sensors, 9(6), Article 6.

Huylenbroeck, L., Laslier, M., Dufour, S., Georges, B., Lejeune, P., & Michez, A. (2020). Using remote sensing to characterize riparian vegetation: A review of available tools and perspectives for managers. Journal of Environmental Management, 267, 110652.

Jabari, S., & Krafczek, M. (2019). Applications of off-nadir satellite imagery in earthquake damage assessment using object-based hog feature descriptor. The International Archives of the Photogrammetry, Remote Sensing and Spatial Information Sciences, XLII-3-W8, 167–171.

Jensen, J.R., 2016. Introductory Digital Image Processing: A remote sensing perspective, 4th ed. Pearson Education, Inc, 1900 E. Lake Ave, Glenview, IL.

Johansen, K., Phinn, S., & Witte, C. (2010). Mapping of riparian zone attributes using discrete return LiDAR, QuickBird and SPOT-5 imagery: Assessing accuracy and costs. Remote Sensing of Environment, 114(11), 2679–2691.

Joshi, C. M., de Leeuw, J., & van Duren, I. C. (2004). Remote sensing and GIS applications for mapping and spatial modelling of invasive species. In ISPRS 2004 : proceedings of the XXth ISPRS congress : Geo-imagery bridging continents, 12-23 July 2004, Istanbul, Turkey. Comm. VII. pp. 669-677 (pp. 669-677). International Society for Photogrammetry and Remote Sensing (ISPRS).

Karakış, S., Marangoz, A. M., & Büyüksalih, G. (2006, February). Analysis of segmentation parameters in eCognition software using high resolution Quickbird MS imagery. In ISPRS Workshop on Topographic Mapping from Space (pp. 14-16).

Kumar Rai, P., & Singh, J. S. (2020). Invasive alien plant species: Their impact on environment, ecosystem services and human health. Ecological Indicators, 111, 106020.

Lehan, N., Murphy, J., Thorburn, L., & Bradley, B. (2013). Accidental introductions are an important source of invasive plants in the continental United States. American Journal of Botany, 100.

Levine, J.M., Vilà, M., D'Antonio, C.M., Dukes, J.S., Grigulis, K. & Lavorel, S. (2003). Mechanisms underlying the impact of exotic plant invasions. Proc. R. Soc. London, Serie B, 270, 775–781.

Lillesand, T., Kiefer, R., Chipman, J., 2015. Remote Sensing and Image Interpretation, 7th ed. Wiley, Hoboken, NJ.

Manfreda, S., McCabe, M., Miller, P., Lucas, R., Pajuelo Madrigal, V., Mallinis, G., Ben Dor, E., Helman, D., Estes, L., Ciraolo, G., Müllerová, J., Tauro, F., De Lima, M. I., De Lima, J. L. M. P., Frances, F., Caylor, K., Kohv, M., Maltese, A., Perks, M., … Toth, B. (2018). On the Use of Unmanned Aerial Systems for Environmental Monitoring [Preprint]. EARTH SCIENCES.

Maxwell, A. E., Warner, T. A., & Fang, F. (2018). Implementation of machine-learning classification in remote sensing: An applied review. International Journal of Remote Sensing, 39(9), 2784–2817.

Mayfield, A. E., Seybold, S. J., Haag, W. R., Johnson, M. T., Kerns, B. K., Kilgo, J. C., Larkin, D. J., Lucardi, R. D., Moltzan, B. D., Pearson, D. E., Rothlisberger, J. D., Schardt, J. D., Schwartz, M. K., & Young, M. K. (2021). Impacts of Invasive Species in Terrestrial and Aquatic Systems in the United States. In T. M. Poland, T. Patel-Weynand, D. M. Finch, C. F. Miniat, D. C. Hayes, & V. M. Lopez (Eds.), Invasive Species in Forests and Rangelands of the United States: A Comprehensive Science Synthesis for the United States Forest Sector (pp. 5–39). Springer International Publishing.

McGlynn, B. L., & Seibert, J. (2003). Distributed assessment of contributing area and riparian buffering along stream networks. Water Resources Research, 39(4).

Michez, A., Piégay, H., Jonathan, L., Claessens, H., & Lejeune, P. (2016). Mapping of riparian invasive species with supervised classification of Unmanned Aerial System (UAS) imagery. International Journal of Applied Earth Observation and Geoinformation, 44, 88–94.

Müllerová, J., Brůna, J., Bartaloš, T., Dvořák, P., Vítková, M., & Pyšek, P. (2017). Timing Is Important: Unmanned Aircraft vs. Satellite Imagery in Plant Invasion Monitoring. Frontiers in Plant Science, 8, 887.

Müllerová, J., Pergl, J., & Pyšek, P. (2013). Remote sensing as a tool for monitoring plant invasions: Testing the effects of data resolution and image classification approach on the detection of a model plant species Heracleum mantegazzianum (giant hogweed). International Journal of Applied Earth Observation and Geoinformation, 25, 55–65.

Naiman, R. J., & Décamps, H. (1997). The Ecology of Interfaces: Riparian Zones. Annual Review of Ecology and Systematics, 28(1), 621–658.

Oswalt, S., Oswalt, C., Crall, A., Rabaglia, R., Schwartz, M. K., & Kerns, B. K. (2021). Inventory and Monitoring of Invasive Species. In T. M. Poland, T. Patel-Weynand, D. M. Finch, C. F. Miniat, D. C. Hayes, & V. M. Lopez (Eds.), Invasive Species in Forests and Rangelands of the United States: A Comprehensive Science Synthesis for the United States Forest Sector (pp. 231–242). Springer International Publishing.

Pimentel, D., Lach, L., Zuniga, R., & Morrison, D. (2000). Environmental and Economic Costs of Nonindigenous Species in the United States. BioScience, 50(1), 53.

Rahe, N. H., Williard, K. W. J., & Schoonover, J. E. (2015). Restoration of Riparian Buffer Function in Reclaimed Surface Mine Soils. JAWRA Journal of the American Water Resources Association, 51(4), 898–909.

Rahman, M., & Saha, S. (2008). Multi-resolution Segmentation for Object-based Classification and Accuracy Assessment of Land Use/Land Cover Classification using Remotely Sensed Data. Journal of the Indian Society of Remote Sensing, 36, 189–201.

Reaser, J. K., Burgiel, S. W., Kirkey, J., Brantley, K. A., Veatch, S. D., & Burgos-Rodríguez, J. (2020). The early detection of and rapid response (EDRR) to invasive species: A conceptual framework and federal capacities assessment. Biological Invasions, 22(1), 1–19.

Rejmánek, M. (2000). Invasive plants: Approaches and predictions. Austral Ecology, 25(5), 497–506.

Richardson, D. M., & Rejmánek, M. (2011). Trees and shrubs as invasive alien species – a global review. Diversity and Distributions, 17(5), 788–809.

Rodriguez-Galiano, V. F., Ghimire, B., Rogan, J., Chica-Olmo, M., & Rigol-Sanchez, J. P. (2012). An assessment of the effectiveness of a random forest classifier for land-cover classification. ISPRS Journal of Photogrammetry and Remote Sensing, 67, 93–104.

Rwanga, S. S., & Ndambuki, J. M. (2017). Accuracy Assessment of Land Use/Land Cover Classification Using Remote Sensing and GIS. International Journal of Geosciences, 08(04), 611.

Saba, F., Valadanzouj, M. J., & Mokhtarzade, M. (2013). The optimization of multi resolution segmentation of remotely sensed data using genetic algorithm. In International Archives of the Photogrammetry, Remote Sensing and Spatial Information Sciences—ISPRS Archives (Vol. 40, p. 349).

Salo, J. A., Theobald, D. M., & Brown, T. C. (2016). Evaluation of methods for delineating riparian zones in a semi-arid montane watershed. Journal of the American Water Resources Association. 52(3): 632-647., 52(3), 632–647.

Sibaruddin, H. I., Shafri, H. Z. M., Pradhan, B., & Haron, N. A. (2018). Comparison of pixel-based and object-based image classification techniques in extracting information from UAV imagery data. IOP Conference Series: Earth and Environmental Science, 169, 012098.

Story, M. and Congalton, R.G. (1986) Accuracy Assessment: A User's Perspective. Photogrammetric Engineering and Remote Sensing, 52, 397-399.

Tian, J., & Chen, D. -M. (2007). Optimization in multi-scale segmentation of high-resolution satellite images for artificial feature recognition. International Journal of Remote Sensing, 28(20), 4625–4644.

Tickner, D. P., Angold, P. G., Gurnell, A. M., & Mountford, J. O. (2001). Riparian plant invasions: Hydrogeomorphological control and ecological impacts. Progress in Physical Geography, 25(1), 22–52.

Tickner, D. P., Angold, P. G., Gurnell, A. M., & Mountford, J. O. (2001). Riparian plant invasions: Hydrogeomorphological control and ecological impacts. Progress in Physical Geography, 25(1), 22–52.

Toth, C., & Jóźków, G. (2016). Remote sensing platforms and sensors: A survey. ISPRS Journal of Photogrammetry and Remote Sensing, 115, 22–36.

Vanderklein, D. W., Galster, J., & Scherr, R. (2014). The impact of Japanese knotweed on stream baseflow. Ecohydrology, 7(2), 881–886.

Verde, N., Mallinis, G., Tsakiri-Strati, M., Georgiadis, C., & Patias, P. (2018). Assessment of Radiometric Resolution Impact on Remote Sensing Data Classification Accuracy. Remote Sensing, 10(8), 1267.

Vidon, P., Allan, C., Burns, D., Duval, T. P., Gurwick, N., Inamdar, S., Lowrance, R., Okay, J., Scott, D., & Sebestyen, S. (2010). Hot Spots and Hot Moments in Riparian Zones: Potential for Improved Water Quality Management1. JAWRA Journal of the American Water Resources Association, 46(2), 278–298.

Vilà, M., & Weiner, J. (2004). Are invasive plant species better competitors than native plant species? – Evidence from pair-wise experiments. Oikos, 105(2), 229–238.

Villarreal, M. L., Van Leeuwen, W. J. D., & Romo-Leon, J. R. (2012). Mapping and monitoring riparian vegetation distribution, structure and composition with regression tree models and post-classification change metrics. International Journal of Remote Sensing, 33(13), 4266–4290.

Westbrooks, R. G. (2004). New Approaches for Early Detection and Rapid Response to Invasive Plants in the United States1. Weed Technology, 18(sp1), 1468–1471.

Xie, Y., Sha, Z., & Yu, M. (2008). Remote sensing imagery in vegetation mapping: A review. Journal of Plant Ecology, 1(1), 9–23.

Yang, X. (2007). Integrated use of remote sensing and geographic information systems in riparian vegetation delineation and mapping. International Journal of Remote Sensing, 28(2), 353–370.